Cell

Presenilin-Dependent Receptor Processing Is Required for Axon Guidance

Ge Bai,[1] Onanong Chivatakarn,[1] Dario Bonanomi,[1] Karen Lettieri,[1] Laura Franco,[1] Caihong Xia,[2] Elke Stein,[3] Le Ma,[2] Joseph W. Lewcock,[1,4] and Samuel L. Pfaff[1,*]

[1]Howard Hughes Medical Institute and Gene Expression Laboratory, The Salk Institute for Biological Studies, 10010 North Torrey Pines Road, La Jolla, CA 92037, USA

[2]Zilkha Neurogenetic Institute, Department of Cell and Neurobiology, Keck School of Medicine, University of Southern California, 1501 San Pablo Street, Los Angeles, CA 90089, USA

[3]Department of Molecular, Cellular, and Developmental Biology, Yale University, 266 Whitney Avenue, New Haven, CT 06520, USA

[4]Present Address: Department of Neurobiology, Genentech, Inc., 1 DNA Way, South San Francisco, CA 94080, USA

*Correspondence: pfaff@salk.edu

DOI 10.1016/j.cell.2010.11.053

SUMMARY

The Alzheimer's disease-linked gene *presenilin* is required for intramembrane proteolysis of amyloid-β precursor protein, contributing to the pathogenesis of neurodegeneration that is characterized by loss of neuronal connections, but the role of Presenilin in establishing neuronal connections is less clear. Through a forward genetic screen in mice for recessive genes affecting motor neurons, we identified the *Columbus* allele, which disrupts motor axon projections from the spinal cord. We mapped this mutation to the *Presenilin-1* gene. Motor neurons and commissural interneurons in *Columbus* mutants lacking Presenilin-1 acquire an inappropriate attraction to Netrin produced by the floor plate because of an accumulation of DCC receptor fragments within the membrane that are insensitive to Slit/Robo silencing. Our findings reveal that Presenilin-dependent DCC receptor processing coordinates the interplay between Netrin/DCC and Slit/Robo signaling. Thus, Presenilin is a key neural circuit builder that gates the spatiotemporal pattern of guidance signaling, thereby ensuring neural projections occur with high fidelity.

INTRODUCTION

Normal behavioral functions rely on complex neural circuits comprised of large ensembles of precisely connected neurons. During embryonic development, the growth of axonal and dendritic processes is tightly regulated to ensure that proper synaptic connections are formed. In the mature nervous system, the growth potential of neurons is generally far less robust; however, some regions of the CNS display ongoing neurogenesis and high levels of plasticity throughout adulthood (Kandel et al., 2000). Although abnormal circuit development and neurodegenerative diseases are both detrimental to the performance of the nervous system, our understanding of the pathways that link the establishment and maintenance of neural circuitries is limited.

Considerable progress has been made in identifying extracellular cues that influence axonal growth cone dynamics, including members of the four classic guidance families: Netrins, Slits, Semaphorins and Ephrins; and their respective neuronal receptors: DCC, Robo, Neuropilins/Plexins and Ephs (Dickson, 2002). Although other guidance factors and receptors continue to be identified, a remarkable feature of these signaling proteins is their recurrent usage throughout the developing nervous system. Moreover, projection neurons extend axons over long distances to their final targets with a series of intermediate guidance cues along their pathway. While this strategy simplifies the problem of locating targets separated by vast distances, it imposes the need for dynamic control of signal responsiveness so that axons do not stall at their intermediate targets (O'Donnell et al., 2009; Tessier-Lavigne and Goodman, 1996; Yu and Bargmann, 2001).

The expression and localization of guidance cues and receptors is exquisitely tailored to allow growth cones to rapidly switch their responsiveness at specific times and places throughout development. Several mechanisms have been identified to ensure the correct presentation and receipt of guidance signals, including regulation of receptor membrane trafficking, endocytosis, proteolytic processing, and localized mRNA transport and translation (Brittis et al., 2002; O'Donnell et al., 2009). Another important strategy for modulating axonal responsiveness derives from the coordinated interplay between different guidance-signaling pathways. For example, Netrin is a chemoattractant for commissural axons until they reach the floor plate (FP) at the midline, where they encounter repulsive Slit ligands. Here Robo becomes activated, triggering repulsion from the midline and silencing the attractive response toward Netrin through direct receptor interaction (Stein and Tessier-Lavigne, 2001). An important remaining challenge has been to understand how different regulatory strategies are coordinated to control the spatial and temporal activity of guidance signaling during embryonic development.

To identify new modulatory components that regulate the spatiotemporal pattern of axon guidance signaling, we performed an ENU mutagenesis screen in transgenic mice using a GFP reporter to visualize embryonic motor neurons (MNs)

(Lewcock et al., 2007). These cells develop within the spinal cord then grow axons into the periphery in a highly stereotypical pattern to form connections with muscles in order to relay locomotor commands. Here, we characterize the *Columbus* mutant, which exhibits a motor axon midline-crossing phenotype, whereby numerous motor axons fail to even exit the neural tube. The *Columbus* mutation disrupts the expression of *Presenilin-1* (*PS1*), which encodes a 467-residue protein with a nine-transmembrane domain topology. PS1 is an essential component of the γ-secretase complex that cleaves amyloid-β precursor protein (APP), leading to the formation of toxic plaques that disrupt neuronal connections and contribute to Alzheimer's disease (AD) pathogenesis. Although multiple embryonically expressed genes including the Notch and DCC receptors have been identified as PS1 substrates, it remains unclear whether PS1 has a role in establishing neuronal connections during development (Parks and Curtis, 2007).

In this study, we show that PS1 function is required to control the spatiotemporal pattern of axonal responses to Netrin by coordinating the activity of different signaling pathways. Our findings reveal an important molecular link between neural circuit formation and disorders causing degeneration.

RESULTS

Columbus Mutants Exhibit Multiple Errors in Motor Axon Guidance

To identify genes involved in motor axon navigation, we conducted a forward genetic screen in GFP reporter mice mutagenized with *N*-ethyl-*N*-nitrosourea (ENU) (Lewcock et al., 2007). The embryonic MN-specific transgenic reporter *ISL^{MN}:GFP-F* was crossed with heterozygous ENU mutants and the offspring were intercrossed to generate homozygous mutants. We identified a mutant we called *Columbus* that displays a severe defect in ventral root formation (Figures S1A–S1D available online) (Lewcock et al., 2007). Normally, motor axons preferentially grow through the anterior half of the somite, whereas *Columbus* motor axons exhibited no preference for the anterior- or posterior-somite, leading to a loss of segmentally organized ventral roots. Transverse sections of *Columbus* mutants also revealed that a subset of MNs had extended axons into the FP rather than out the ventral roots (Figures 1A, 1B, 1D, and 1E). To characterize the midline axon growth defect in more detail, we imaged spinal cords using an open book preparation at E13 and found MN misprojections at all levels of the spinal cord (Figures 1G, 1H, 1J, and 1K and data not shown). Some motor axons crossed the midline and projected to the contralateral side while others stalled in the FP and formed bundles (Figures S1E and S1F). Likewise, midline motor axon guidance defects were observed with other MN reporters such as *Hb9:GFP* (Figures S1G and S1H).

Presenilin-1 (*PS1*) Is Mutated in *Columbus*

SNP markers for the mutagenized DBA mouse strain were used to map the *Columbus* mutation to a 16.7 Mb segment on chromosome 12. The ventral root segmentation and midline-crossing motor axon phenotypes did not segregate during the outcrosses. Next, genomic DNA for candidate genes was sequenced. We identified a Thymine to Adenine base conversion in intron 11 of the mouse *presenilin-1* gene (*PS1*), which has 12 exons and 11 introns in the genome (Figure 1M and Figures S1I and S1J). To examine how this mutation affects PS1 expression, we first performed RT-PCR on *PS1* mRNA from *Columbus* mutants using primers that flank the 11th intron. We found that the point mutation shifted the PCR product from 164 bp to 401 bp in *Columbus* mutants (Figure 1N). Sequencing *Columbus* mutant *PS1* transcripts showed that the T/A base conversion disrupted the normal splice site for the 12th exon of *PS1.* The mutation unmasked a cryptic splice acceptor within intron 11 that resulted in a 237 bp insertion, which introduces two premature stop codons (Figure 1M). Western-blot analysis revealed that PS1 protein was undetectable in *Columbus* mutants using both anti-N and -C-terminal antibodies. These findings demonstrate that the *Columbus* mutation alters *PS1* splicing, which severely disrupts PS1 protein expression (Figure 1O).

To confirm that the motor axon guidance defects observed in *Columbus* mutants were due to PS1 rather than another mutation, we crossed the *ISL^{MN}:GFP-F* MN reporter into *PS1* knockout mice (Shen et al., 1997). Embryos with a targeted disruption of the *PS1* gene displayed a similar combination of pathfinding errors to those observed in the *Columbus* mutant, including failure to form discrete ventral roots and midline-crossing of motor axons (Figures 1C, 1F, 1I, 1L; Figures S1K–S1P; and data not shown). Next we analyzed the distribution of PS1 protein in mouse embryos using immunofluorescence and found it was expressed at high levels by MNs and interneurons in the spinal cord as well as peripheral tissues (Figures S2A–S2C). In contrast, progenitor cells in the ventricular zone expressed much lower levels of PS1. Within MNs PS1 was detected as the cells became postmitotically born and began axonogenesis, and both cell bodies and axons were labeled.

PS1 Function in Cell Fate Specification

Based on the expression of PS1, it remained unclear whether it was required for spinal neuron differentiation, motor axon guidance, and/or the proper development of peripheral tissues. Notch-delta signaling is required for both spinal cord neurogenesis and somite development, and cleavage of the Notch receptor by γ-secretase is required to generate the notch intracellular domain involved in gene regulation (Selkoe and Kopan, 2003). To determine which tissues require PS1 activity, we crossed floxed *PS1* mice with *Nestin-Cre* transgenic mice to generate a neural cell-specific *PS1* conditional knockout (*PS1* cKO) mouse. In *PS1* cKO embryos, the segmentally repeated ventral roots developed normally (data not shown), whereas the inappropriate midline-crossing motor axon tracts still formed (Figures S2D and S2E). These data suggest that nonneuronal expression of PS1 is required for proper ventral root formation, likely because PS1 is necessary for anteroposterior somite patterning (Shen et al., 1997). In contrast, the midline motor axon-crossing defect in *PS1* mutants arises from defects within the neural tube.

Next, we examined progenitor cell growth and neural differentiation in developing spinal cords from *Columbus* mutants using immunofluorescent staining. We found that loss of PS1 function did not change progenitor cell patterning, MN specification, or MN subtype diversification (Figures S2F–S2K), presumably because PS2 can partially compensate for PS1 inactivation in

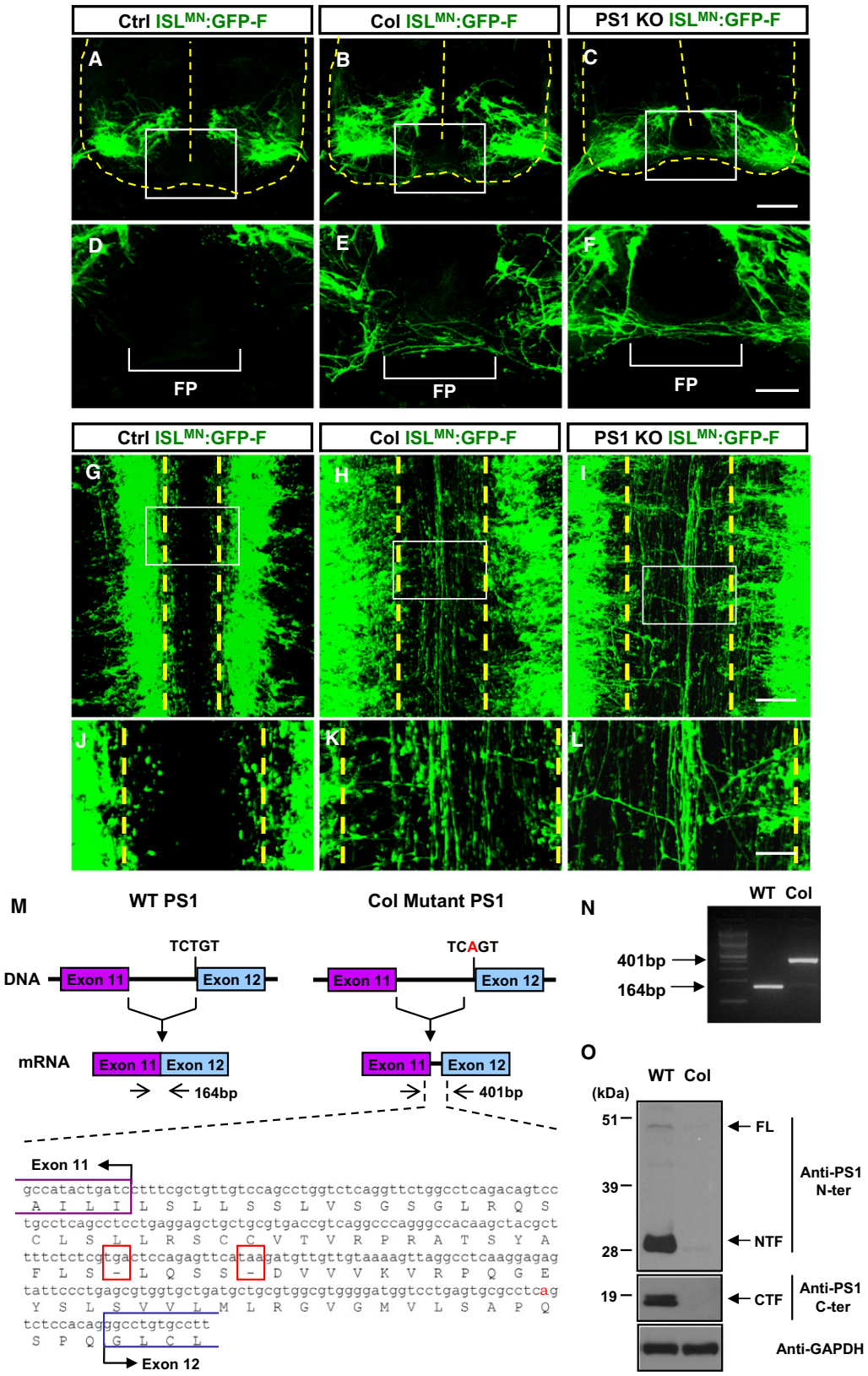
Ctrl ISL^MN:GFP-F
Col ISL^MN:GFP-F
PS1 KO ISL^MN:GFP-F
A
B
C
D
E
F
FP
FP
FP
Ctrl ISL^MN:GFP-F
Col ISL^MN:GFP-F
PS1 KO ISL^MN:GFP-F
G
H
I
J
K
L
M
WT PS1
Col Mutant PS1
DNA
TCTGT
TCAGT
Exon 11
Exon 12
Exon 11
Exon 12
mRNA
Exon 11
Exon 12
164bp
Exon 11
Exon 12
401bp
Exon 11
gccatactgatcctttcgctgttgtccagcctggtctcaggttctggcctcagacagtcc
A I L I L S L L S S L V S G S G L R Q S
tgcctcagcctcctgaggagctgctgcgtgaccgtcaggcccagggccacaagctacgct
C L S L L R S C C V T V R P R A T S Y A
tttctctcgtgactccagagttcataagatgttgttgtaaaagttaggcctcaaggagag
F L S - L Q S S - D V V V K V R P Q G E
tattccctgagcgtggtgctgatgctgcgtggcgtggggatggtcctgagtgcgcctcag
Y S L S V V L M L R G V G M V L S A P Q
tctccacaggggcctgtgccttg
S P Q G L C L
Exon 12
N
WT Col
401bp
164bp
O
WT Col
(kDa)
51
39
28
19
FL
NTF
CTF
Anti-PS1 N-ter
Anti-PS1 C-ter
Anti-GAPDH

maintaining Notch signaling (Donoviel et al., 1999). Taken together, our results indicate that the midline motor axon growth defect is due to a neural-tube-intrinsic function of PS1 that is unrelated to MN fate specification.

Motor Axons Grow Toward the Floor Plate in *PS1* Mutants

Since the inappropriate midline-growth of motor axons was intrinsic to the neural tube, we tested whether the FP and/or MNs behaved abnormally in *PS1* mutants. The FP and GFP-labeled MNs were dissected from *ISL^{MN}:GFP-F* E12 embryos. Tissue was taken separately from either *PS1* knockout mutants or controls (a mix of heterozygous and wild-type embryos) and cocultured in 3D collagen/matrigel matrices for 24 hr. A semi-quantitative assessment of axon outgrowth was performed by counting GFP-positive neurite numbers on the side facing toward (proximal) and away (distal) from the FP (Figure 2A).

In the presence of control FP explants, MNs from wild-type embryos extended more axons from the distal side of the explant, indicating the FP either represses or repels motor axon growth (Figures 2C and 2G). Likewise, control MNs failed to extend axons toward FP explants dissected from *PS1* mutant embryos (Figures 2E and 2G). On the other hand, MNs dissected from *PS1* mutant embryos extended numerous axons toward FP explants regardless of whether the FP was dissected from control or PS1-deficient embryos (Figures 2D, 2F, and 2G). Thus, PS1 inactivation in FP cells does not alter motor axon growth compared to controls, whereas the loss of PS1 function in neural tissue leads to aberrant growth of MNs in explant cultures. These findings indicate that PS1-deficient MNs either lose responsiveness to a chemorepellent from the FP or acquire responsiveness to a chemoattractant.

PS1-Deficient Motor Neurons Are Attracted to Netrin-1

To examine whether *PS1* mutant MNs displayed abnormal responsiveness to guidance signals, we cocultured GFP-labeled MN explants from *ISL^{MN}:GFP-F* embryos with Cos cell aggregates that had been transfected with cDNAs encoding known guidance signals. Since Semaphorins are well-established repellents in the midline, we tested whether MN responsiveness to Sema3A was altered in *PS1* mutants. We found that both control and PS1-deficient MNs were repelled by Cos cell aggregates expressing Sema3A after 24 hr in culture (Figures 2H–2L). Neither wild-type nor PS1-deficient spinal MNs from E12 embryos were repelled by Slit2-secreting cell clusters (Figure 2L), suggesting that midline-growth of *PS1* mutant MNs is not due to loss of Slit responsiveness.

To assess whether MN attraction to guidance signals was altered, we shortened our coculture assay to 15–18 hr to minimize axonal outgrowth in the absence of growth-promoting signals (Figure 2B). We first tested Shh and Netrin-1, which are both known chemoattractants expressed by the FP (Charron et al., 2003; Kennedy et al., 1994). Neither control nor PS1-deficient MNs were attracted to Cos cells secreting Shh (Figures 2O and 2P). Likewise, Netrin-1 failed to promote axonal outgrowth from control MNs (Figure 2Q). Interestingly, there was a marked increase in axonal outgrowth from *PS1* mutant explants when co-cultured with Netrin-1 secreting Cos cells (Figure 2R). To exclude the possibility that Netrin-1 acted indirectly by altering the Cos cell aggregates, we tested whether purified recombinant Netrin-1 was active. We found that MN explants from control embryos were unresponsive, whereas explants from *PS1* mutants extended axons in a dose-dependent manner to bath-applied recombinant Netrin-1 (Figure 2T). These results suggest that *PS1* mutant MNs acquire abnormal responsiveness to Netrin-1.

Inhibition of Netrin-1/DCC Signaling Rescues the Midline-Motor Axon Phenotype

To test whether abnormal Netrin responsiveness caused motor axon guidance defects, we crossed *PS1* knockout mice to *Netrin-1* hypomorphic mutants to generate *PS1/Netrin-1* double-mutant embryos (Serafini et al., 1996). We found that the inappropriate growth of motor axons within the FP was significantly reduced by disruption of Netrin-1 expression (Figures 3D–3I). Next, we tested whether DCC was required for PS1-deficient MN chemoattraction to the FP. The axon outgrowth from *PS1* mutant MNs toward FP explants was inhibited by function blocking antibodies to DCC (Figures 3A–3C). Furthermore, we found that MNs in *PS1/DCC* double-knockout embryos avoided the FP (Figures 3J–3O). These data suggest that MNs lacking PS1 become attracted to Netrin-1 because of abnormal signaling from the DCC receptor, which leads to inappropriate motor axon growth into the FP.

Inhibition of γ-Secretase Activity Confers Responsiveness to Netrin

PS1 encodes the catalytic component of the multisubunit γ-secretase, but it was unclear whether protease activity was required for regulating MN axon growth. We added γ-secretase antagonist L-685458 to wild-type explant cultures and assayed motor

Figure 1. *Columbus* Mutants Display Midline Motor Axon Guidance Defects

(A–F) Motor axons in transverse sections of E12.5 mouse embryos at the brachial level labeled with *ISL^{MN}:GFP-F* transgenic reporter. Boxed regions in (A–C) are enlarged in (D–F), respectively. n > 8 embryos for each genotype.

(G–L) Flat-mount images of E13 mouse spinal cords at lumbar levels with anterior on top. Boxed regions in (G–I) are enlarged in (J–L), respectively. Dotted line marks medial edge of MN cell bodies. Note that motor columns are slightly disorganized at the lumbar level of *PS1* mutants, leading to an increased distance between the motor columns. n > 10 embryos for each genotype.

(M) Schematic of *Columbus* mutation in *PS1* gene.

(N) RT-PCR analysis of *PS1* mRNA using primers flanking intron 11 (arrowheads in M).

(O) Western-blot analysis of PS1 protein in *Columbus* mutants. Full-length PS1 protein is proteolytically processed in vivo to a 30 kDa N-terminal fragment (NTF) and a 20 kDa C-terminal fragment (CTF). Antibody against PS1 N terminus recognized the full-length holoprotein (FL) and NTF in wild-type but not in the *Columbus* mutant. Likewise, an antibody against the C terminus of PS1 recognized the 20 kDa CTF in wild-type but not *Columbus* mutants. GAPDH was used as an internal control.

The scale bars represent 100 μm (A–C), 40 μm (D–F), 75 μm (G–I), and 30 μm (J–L). See also Figure S1.

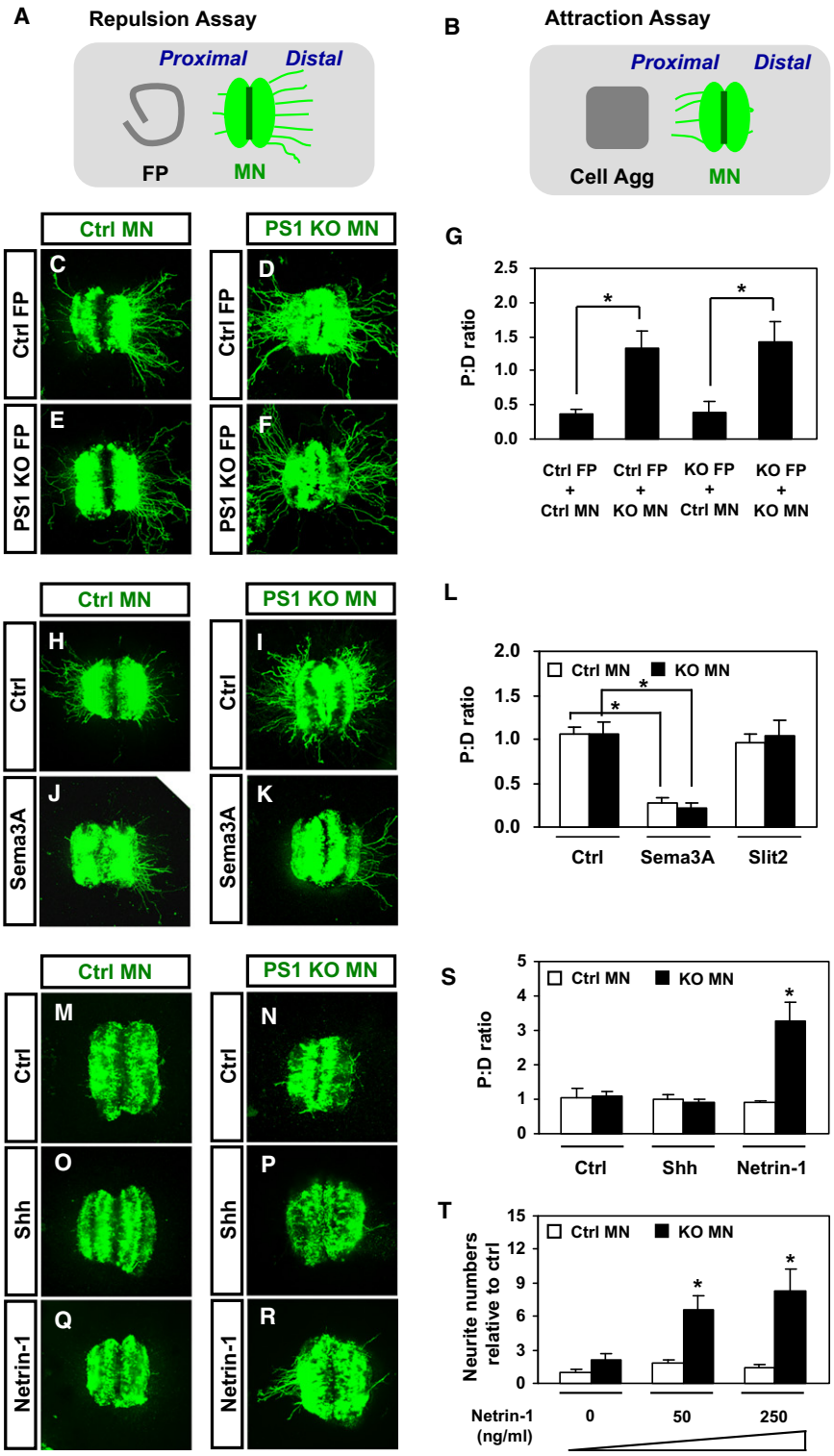

Figure 2. PS1-Deficient Motor Neurons Are Attracted to Netrin

(A) Schematic of motor explant repulsion assay. MN explants are cocultured with floor plate or Cos cell aggregates in 3D collagen/matrigel matrices for 24 hr. Motor axons are visualized with the transgenic *ISL*^{MN}*:GFP-F* reporter.

(B) Schematic of motor explant attraction assay. MN explants are cocultured with Cos cell aggregates (Cell Agg) in 3D collagen/matrigel matrices for 15 hr, which is insufficient time for motor axon outgrowth unless the Cos cells express a chemoattractant.

(C–F) Motor explant repulsion assay. GFP-labeled mouse motor explants were cocultured with FP (FP was to the left of explants). FPs and motor explants from *PS1* heterozygous or wild-type littermates were used as controls.

(G) Histogram showing quantification (proximal:distal [P:D] ratio) of outgrowth from explants in culture with FPs. n = 8 (Ctrl FP + Ctrl MN), n = 7 (Ctrl FP + KO MN), n = 7 (KO FP + Ctrl MN), n = 5 explants (KO FP + KO MN). Data are presented as the mean ± standard error of the mean (SEM) (*$p < 0.05$). The following abbreviations are used: Ctrl, control; KO, knockout.

(H–K) Motor explant repulsion assay. GFP-labeled mouse motor explants were cocultured with Cos cell aggregates and transfected as indicated (cell aggregates were to the left of explants).

(L) P:D ratio of outgrowth from explants in the presence of cell aggregates. For control (wild-type/heterozygous [WT/Het]) motor explants, n = 13 (control), n = 10 (Sema3A), n = 17 (Slit2); for *PS1* KO motor explants, n = 9 (control), n = 11 (Sema3A), n = 9 (Slit2). Data are presented as the mean ± SEM (*$p < 0.05$).

(M–R) Motor explant attraction assay. GFP-labeled mouse motor explants were cocultured with Cos cell aggregates transfected as indicated (cell aggregates were to the left of explants).

(S) P:D ratio of outgrowth from explants in the presence of Cos cell aggregates. For control (WT/Het) motor explants, n = 11 (control), n = 10 (Shh), n = 12 (Netrin); for *PS1* KO motor explants, n = 15 (control), n = 8 (Shh), n = 10 (Netrin). Data are presented as the mean ± SEM (*$p < 0.05$).

(T) Histogram showing quantification (neurite numbers relative to control) of outgrowth from motor explants in the presence of recombinant Netrin-1. For control (WT/Het) motor explants, n = 21 (0 ng/ml), n = 25 (50 ng/ml), n = 19 (250 ng/ml); for *PS1* KO motor explants, n = 13 (0 ng/ml), n = 15 (50 ng/ml), n = 16 (250 ng/ml). Data are presented as the mean ± SEM (*$p < 0.05$). See also Figure S2.

axon responses to recombinant or Cos cell produced Netrin-1. Netrin-mediated motor axon growth was stimulated when L-685458 was added to the medium (Figures 4A and 4B and data not shown), indicating that the catalytic activity of PS1 is normally required to prevent MNs from responding to Netrin-1. Furthermore, the finding that MNs become responsive to

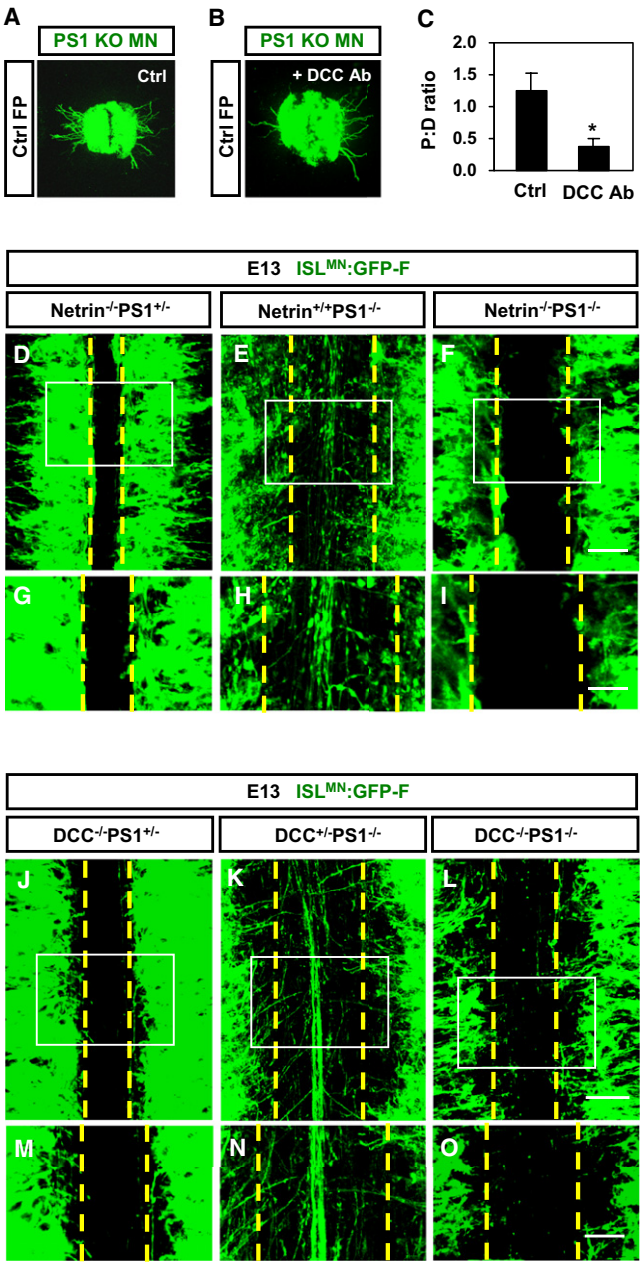

Figure 3. Inhibition of Netrin/DCC Signaling Rescues the Midline-Crossing Phenotype

(A and B) Motor explant repulsion assay. GFP-labeled *PS1* KO motor explants were cocultured with control (WT/Het) FPs in the presence of (A) vehicle control or (B) DCC function-blocking antibody.

(C) P:D ratio of outgrowth from explants in the presence of FPs. n = 9 (control), n = 7 (DCC Ab). Data are presented as the mean ± SEM (*$p < 0.05$).

(D–O) Flat-mount images of GFP-positive MNs in E13 lumbar mouse spinal cords. Boxed regions in (D–F) and (J–L) are enlarged in (G–I) and (M–O), respectively. Anterior is to the top for all the images. Note that motor columns are slightly disorganized in *PS1/Netrin-1* and *PS1/DCC* double mutants, similar to those observed in *PS1* single mutants. At least three embryos were assayed for each genotype. The scale bars represent 50 μm (D–F), 30 μm (G–I), 50 μm (J–L), and 30 μm (M–O).

Netrin-1 following the acute inhibition of PS1 activity with L-685458 suggests that the axon guidance defects in *PS1* mutants are not indirectly due to developmental defects that arise from the chronic loss of γ-secretase activity throughout embryonic development.

Next we tested whether isolated MNs lacking γ-secretase activity turn in response to Netrin-1. We established a Dunn chamber assay to create a Netrin-1 gradient (Yam et al., 2009). In this assay, the outer annular well was filled with media containing Netrin-1, and the inner well was filled with control media (Figure 4D). A gradient was formed over the annular bridge through diffusion of the Netrin from the outer to the inner well that was stable for many hours (Yam et al., 2009) (data not shown). *ISL^{MN}:GFP*-positive (wild-type) chick MNs were dissociated and cultured on a coverslip, which was then inverted over the Dunn chamber (Figures 4D and 4E). In the control condition, the direction of motor axonal growth remained unchanged (Figure 4F). In contrast, when γ-secretase inhibitor L-685458 was added axons turned toward the source of Netrin-1 (Figure 4G). To quantify the extent of turning, we measured the initial angle (α), defined as the angle between the initial orientation of the axon and the gradient, and the angle turned (β), defined as the angle between the initial and final trajectories of the axon (positive for turns up the gradient and negative for turns down the gradient) (Yam et al., 2009) (Figure 4H). Scatter plots of these angles showed that for the control condition, no net turning occurred. However, in the presence of γ-secretase inhibitor, there was a significant bias toward positive turning angles (Figures 4I and 4J). Together, these data indicate that γ-secretase activity is required cell autonomously for newly generated MNs to prevent the Netrin receptor expressed by MNs from responding to Netrin-1 as a chemoattractant.

DCC Stubs Promote Axon Growth

Next we explored how γ-secretase was involved in regulating MN responsiveness to Netrin. Previous studies have found that DCC is the target of protease cleavage (Taniguchi et al., 2003). First, DCC is cleaved by metalloprotease(s) that lead to shedding of the ectodomain segment, generating a membrane-tethered DCC stub. This DCC stub is the substrate of γ-secretase, which releases the intracellular domain (ICD) from the membrane (Figure 5A) (Taniguchi et al., 2003). Although the full-length DCC receptor is typically viewed as the primary Netrin-signaling component, it has been shown that the DCC stub and DCC-ICD also have signaling properties (Gitai et al., 2003; Parent et al., 2005; Taniguchi et al., 2003). We found that the levels of DCC stubs and DCC-ICD fragments were very low in wild-type neurons, whereas DCC stubs accumulated to high levels in *PS1* mutants (Figures 5B and 5C and data not shown). As expected, γ-secretase inhibition also caused the DCC stub to accumulate (see below). To examine whether cleavage of DCC played a role in Netrin signaling in MNs we performed collagen assays with wild-type MN explants and Netrin-1-producing cells in the presence or absence of metalloprotease and/or γ-secretase inhibitors. Application of metalloprotease inhibitor GM6001 failed to stimulate motor axon outgrowth, while the γ-secretase inhibitor L-685458 caused motor axons to become responsive to Netrin-1 (Figures 5D–5F and 5H). Interestingly, the

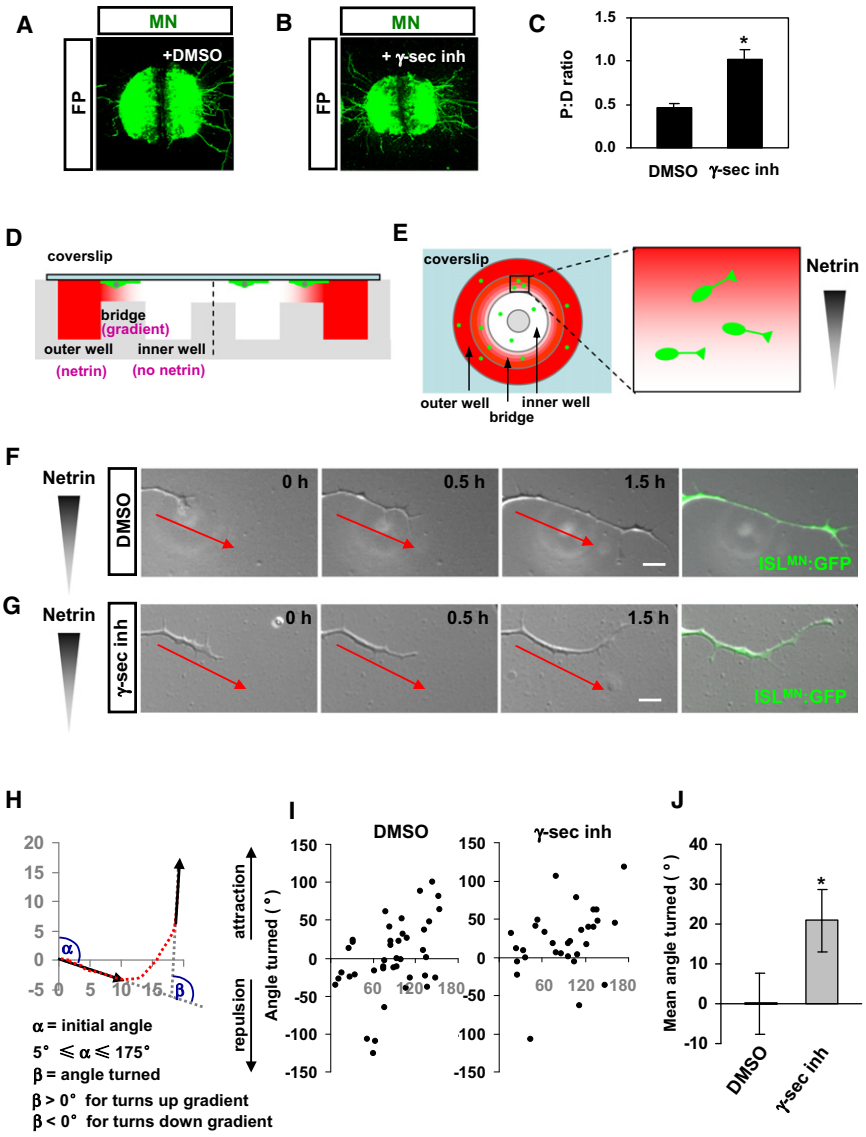

Figure 4. Inhibition of γ-Secretase Activity Switches MNs to a Netrin-Responsive State

(A and B) Motor explant repulsion assay. GFP-labeled motor explants were cocultured with FPs in the presence of (A) DMSO vehicle or (B) γ-secretase inhibitor L-685458.

(C) P:D ratio of outgrowth from explants in the presence of FPs. n = 7 (DMSO), n = 9 (γ-sec inh). Data are presented as the mean ± SEM (*$p < 0.05$).

(D) Side view and (E) top view schematic of an assembled Dunn chamber. ISL^{MN}:GFP-labeled chick MNs cultured on a coverslip have been inverted over the chamber. The inner well is filled with control media, whereas the outer well is filled with media containing 50 ng/ml of Netrin-1. A gradient forms across the annular bridge because of diffusion of Netrin-1 from the outer to the inner well.

(F) In the presence of DMSO, growing chick MNs did not change their trajectories in the Netrin gradient.

(G) In the presence of γ-secretase inhibitor, motor axons turned toward increasing concentrations of Netrin. Note that all images have been rotated such that the gradient increases along the *y* axis. The scale bar represents 10 μm.

(H) Definition of the initial angle, α, the angle between the initial axon position and the gradient, and angle turned, β, the angle between the vectors representing the initial and final positions of the axon. The first and last 10 μm of the axons were tracked to obtain trajectories.

(I) Scatter plot of the angle turned versus the initial angle for motor axons in the presence of dimethyl sulfoxide (DMSO) or γ-secretase inhibitor (γ-sec inh) L-685458. n = 41 (DMSO), n = 31 (γ-sec inh).

(J) Histogram showing the mean angle turned (± SEM) for axons in the presence of DMSO or γ-secretase inhibitor L-685458. (*$p < 0.05$; Kolmogorov-Smirnov test).

addition of GM6001 to the culture blocked the ability of L-685458 to trigger MN chemoattraction to Netrin-1, indicating that metalloprotease-mediated cleavage is a prerequisite for acquiring Netrin responsiveness (Figures 5G and 5H). Thus, full-length DCC is unlikely to be sufficient to cause MN chemoattraction. Taken together, these data suggest that DCC in MNs is normally the target of a sequential protease pathway.

Blocking γ-secretase activity should have two effects on DCC processing: (1) cause an accumulation of membrane-tethered DCC stubs, and (2) reduce the generation of DCC-ICD fragments (Figure 5A and 5B). To test whether one or both of these DCC fragments influenced motor axon growth, we made two constructs, one containing the intracellular domain of DCC (DCC-ICD) and the other containing a myristoylated form of the intracellular domain of DCC (Myr-DCC-ICD) to mimic membrane-tethered DCC stubs. First, Myr-DCC-ICD was coelectroporated into Hamburger-Hamilton (HH) stage 14 chick embryo neural tubes with a MN-specific reporter *Hb9:DsRed*. After 2 days incubation, the spinal cords were flat mounted and imaged. We found that the Myr-DCC-ICD construct mimicking DCC stubs induced DsRed-positive motor axons to cross the midline and project contralaterally like MNs in *PS1* mouse mutants (Figures 5I and 5J). In contrast, expression of: (1) DCC full-length receptor, (2) the DCC extracellular domain, and (3) the DCC-ICD each failed to induce motor axon growth toward the FP (Figures 5K–5M).

Next we tested whether a loss of DCC-ICD signaling caused MNs lacking γ-secretase activity to become responsive to Netrin-1. MN explants were dissected from Hb9:DsRed electroporated chick embryos and cocultured with Cos cells expressing Netrin-1. Wild-type DsRed-positive MNs were not attracted to Netrin-1, whereas explants treated with the γ-secretase inhibitor L-685458 became Netrin-1 responsive (Figures 5N, 5P, and 5R). This finding suggests that Netrin receptor regulation by γ-secretase is evolutionarily conserved in chick. Likewise, MNs were

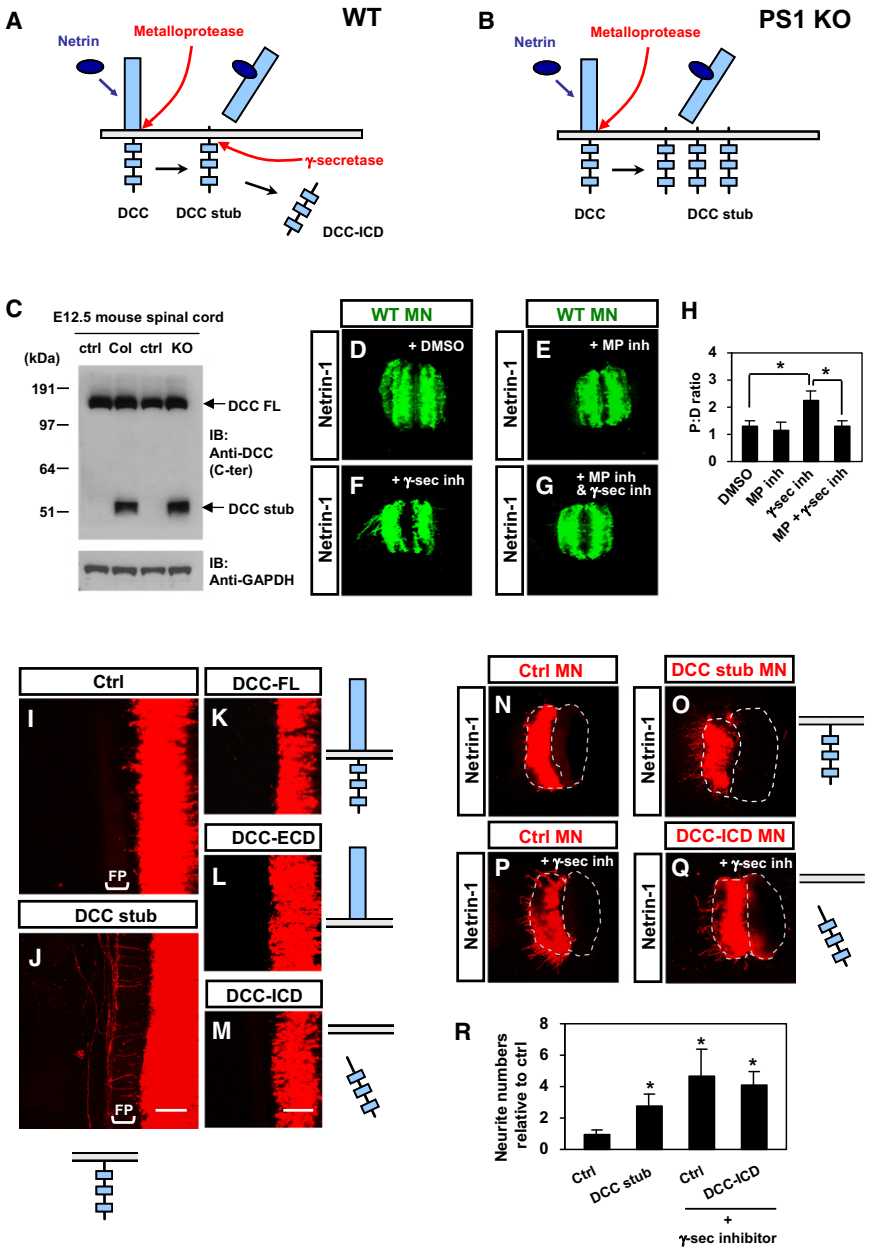

Figure 5. DCC Stubs Cause Motor Neuron Chemoattraction to Netrin

(A) In wild-type embryos, DCC is first cleaved by a metalloprotease that leads to shedding of the ectodomain segment, generating membrane-tethered DCC stubs. DCC stub is subsequently processed by γ-secretase to generate ICD. (B) In *PS1* KO embryos, the production of DCC-ICD is disrupted, and DCC stubs accumulate to high levels on the cell membrane.

(C) Western-blot analysis of DCC protein in mouse spinal cords. Protein extracts from the spinal cords of *Columbus* mutants (Col, lane 2), *PS1* knockouts (KO, lane 4), or their control littermates (Ctrl, lane 1 and 3) were analyzed by immunoblotting with the DCC intracellular domain-specific antibody. High levels of DCC stub were apparent in *Columbus* and *PS1* KO embryos. Glyceraldehyde 3-phosphate dehydrogenase (GAPDH) was used as an internal standard.

(D–G) Motor explant attraction assay. GFP-labeled mouse motor explants were cocultured with Netrin-1 cell aggregates in the presence of (D) DMSO vehicle, (E) metalloprotease inhibitor GM6001, (F) γ-secretase inhibitor L-685458, or (G) both GM6001 and L-685458.

(H) P:D ratio of outgrowth from mouse motor explants in the presence of Netrin-1 cell aggregates. n = 16 (DMSO), n = 8 (metalloprotease inhibitor [MP inh]), n = 20 (γ-sec inh), and n = 19 explants (MP inh + γ-sec inh). Data are presented as the mean ± SEM (*$p < 0.05$).

(I–M) Flat-mount images of chick spinal cords that have been electroporated with plasmids encoding myristoylated DCC intracellular domain (DCC stub), DCC full-length (DCC-FL), DCC extracellular domain (DCC-ECD), or DCC intracellular domain (DCC-ICD) as indicated. Hb9-DsRed reporter (red) was coelectroporated to label MNs. n > 8 embryos for each plasmid. The scale bar represents 100 μm.

(N–Q) Chick motor explant attraction assay. Chick spinal cords were electroporated with plasmids encoding myristoylated DCC intracellular domain (DCC stub), DCC intracellular domain (DCC-ICD), or control plasmids as indicated. Hb9:DsRed reporter (red) was coelectroporated to label MNs. Motor explants were dissected from electroporated spinal cords and cocultured with the Netrin-1 cell aggregates in 3D collagen/matrigel matrices for 15 hr. Minimal axon outgrowth was observed from MNs in control conditions.

(R) Histogram showing quantification (neurite numbers relative to control) of outgrowth from chick motor explants in the presence of Netrin-1 cell aggregates. n = 16 (control), n = 13 (DCC stub), n = 9 (control + L-685458), and n = 14 (DCC-ICD + L-685458). Data are presented as the mean ± SEM (*$p < 0.05$).

attracted to Netrin-1 when electroporated with Myr-DCC-ICD (DCC stub mimic) (Figures 5O and 5R). Electroporation of the DCC-ICD failed to prevent L-685458-treated MNs from responding to Netrin-1 (Figures 5Q and 5R), suggesting that inappropriate Netrin attraction is not due to an inability to generate the intracellular domain fragments in *PS1* mutants. Rather, these data indicated that the accumulation of DCC stubs in *PS1* mutants cause newly generated MNs to become responsive to Netrin-1 in the FP.

Inhibition of Slit/Robo Signaling Switches Motor Neurons to a Netrin-1 Responsive State

Since MNs express high levels of DCC (Figures S3A and S3B and data not shown) (Keino-Masu et al., 1996), we wondered what normally prevents these neurons from growing to the Netrin-positive FP. Growth cone turning assays suggest that commissural neurons silence Netrin signaling when their axons encounter the Slit-expressing FP, which activates the Robo receptor and leads to Robo-DCC interactions that prevent Netrin

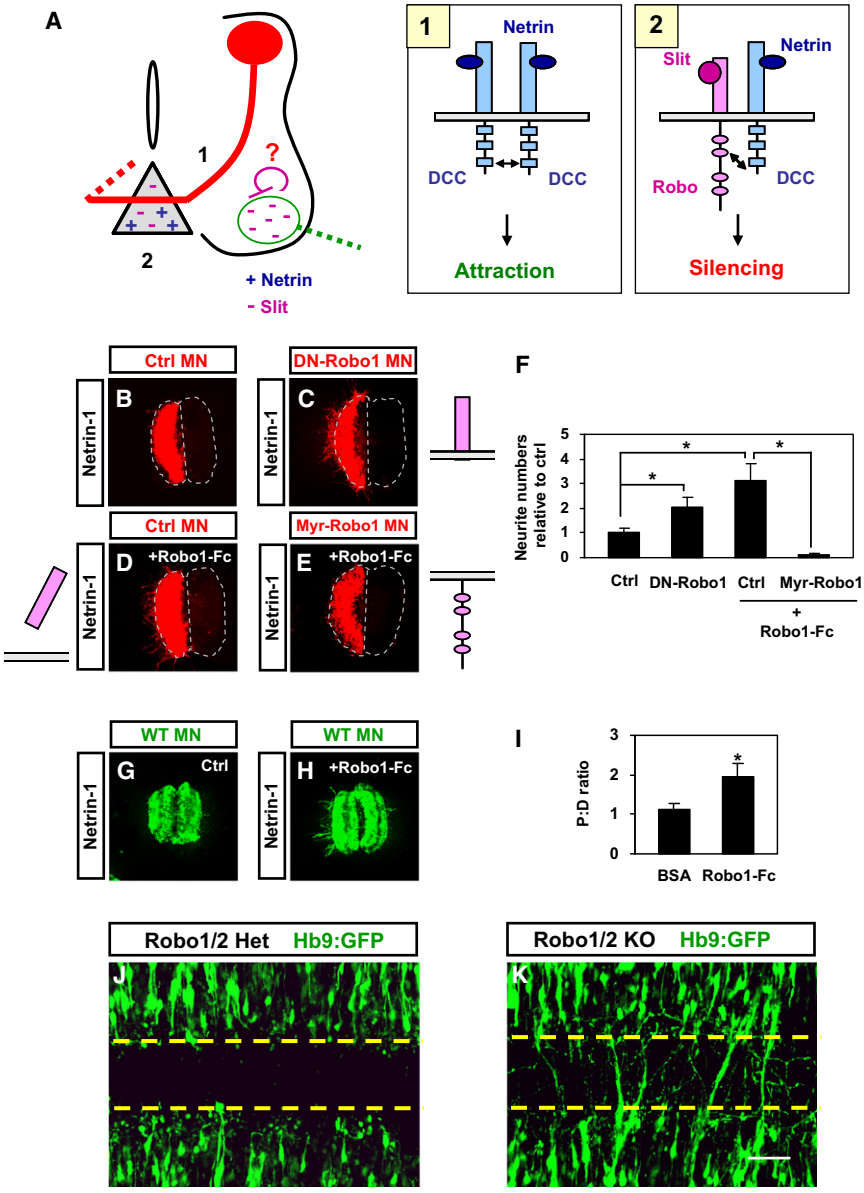

Figure 6. Inhibition of Slit/Robo Signaling Induces Motor Axon Growth Toward Netrin-1

(A) Spinal cord diagram showing Slit/Robo-mediated silencing mechanism. (1) Pre-crossing commissural axons (red) are attracted to the FP (gray triangle) by Netrin (+) receptor DCC; (2) the midline Slit (–) activates Robo which blocks Netrin/DCC attraction. Slit is expressed in the motor column (green circle), leading to the possibility of a self-silencing mechanism that inhibits Netrin responsiveness in MNs.

(B–E) Chick motor explant attraction assay. Chick spinal cords have been electroporated with plasmids encoding Robo1 extracellular domain (DN-Robo1), myristoylated Robo1 intracellular domain (Myr-Robo1), or control plasmids as indicated. Hb9:DsRed (red) reporter was coelectroporated with above plasmids to label MNs.

(F) Histogram showing quantification (neurite numbers relative to control) of outgrowth from chick motor explants in the presence of Netrin-1 cell aggregates. n = 13 (control), n = 8 (DN-Robo1), n = 10 (control + Robo1-Fc), and n = 10 (Myr-Robo1 + Robo1-Fc). Data are presented as the mean ± SEM (*$p < 0.05$).

(G and H) Motor explant attraction assay. Mouse motor explants were cocultured with Netrin-1 cell aggregates in the presence of vehicle control or Robo1-Fc.

(I) P:D ratio of outgrowth from motor explants in the presence of Netrin-1 cell aggregates. n = 16 (BSA) and n = 19 (Robo1-Fc). Data are presented as the mean ± SEM (*$p < 0.05$).

(J and K) Flat-mount images of E13.5 mouse spinal cords at lumbar levels with anterior on the left. Dotted line marks medial edge of MN cell bodies. At least five embryos were assayed for each genotype.

See also Figure S3.

attraction (Figure 6A) (Stein and Tessier-Lavigne, 2001). Interestingly, MNs coexpress both Slit and Robo (Figures S3C–S3F) (Brose et al., 1999), leading to the possibility of a self-silencing mechanism that inhibits Netrin responsiveness (Figure 6A). To test this hypothesis, we cocultured chick DsRed-positive MN explants with Netrin-1 expressing Cos cell aggregates. Wild-type chick MNs are normally not attracted to Netrin, but electroporation of a dominant-negative form of Robo1 (Robo1-ectodomain + transmembrane domain) into the explants induced motor axon growth toward the Netrin-1 source (Figures 6C and 6F). A similar effect was observed when Robo1-Fc was bath-applied to the explants to sequester Slits (Figures 6D and 6F). Next we generated a gain-of-function variant of Robo1 by combining a myristoylation signal to the intracellular domain of Robo1 (Myr-Robo1), which has been demonstrated to constitutively interact with the DCC cytoplasmic domain (Stein and Tessier-Lavigne, 2001). Electroporation of Myr-Robo1 into chick MNs markedly inhibited the attraction to Netrin-1 caused by Robo1-Fc (Figures 6E and 6F). A similar effect was observed in mouse explants in which bath-applied Robo1-Fc induced motor axon growth toward Netrin-1 (Figures 6G and 6H). To confirm these observations in vivo, we crossed *Robo1/2* double mutants to MN transgenic reporter *Hb9:GFP* and found a subset of MNs extended axons into the FP (Figures 6J and 6K). These findings suggest MNs normally use a self-silencing mechanism based on Slit/Robo coexpression to prevent DCC from causing attraction to Netrin produced by the FP.

DCC Stubs Are Immune to Robo-Mediated Silencing

Next we examined why the Slit/Robo silencing of Netrin-chemoattraction was ineffective in *PS1* mutants. Since DCC stubs accumulate in PS1-deficient embryos, first we tested whether

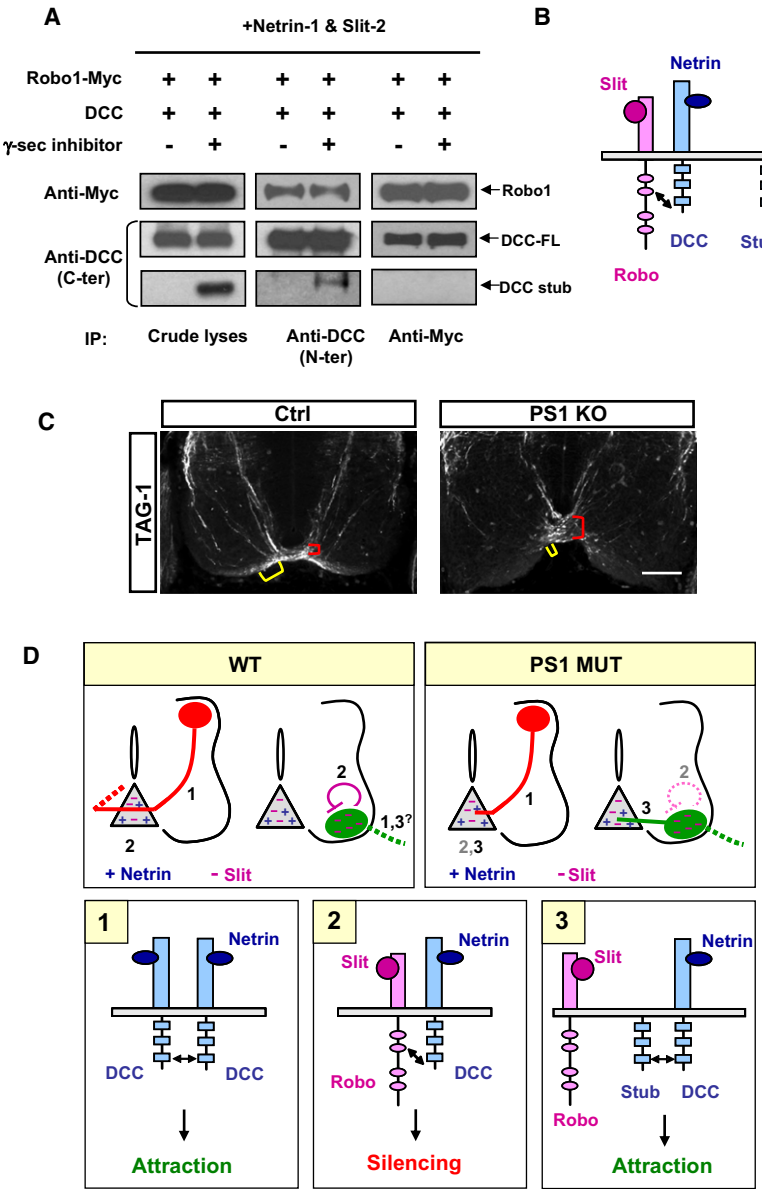

Figure 7. DCC Stubs Do Not Interact with Robo

(A) Interaction of Robo and DCC in 293-T cells cotransfected with plasmids encoding Robo1-Myc and DCC. Sixteen hours after transfection, cells were treated with vehicle DMSO or γ-secretase inhibitor for an additional 10 hr, then incubated for 20 min with recombinant Netrin-1 and Slit2 and subjected to immunoprecipitation (IP) with antibodies to Myc or DCC extracellular domain (N-ter). Immunoprecipitates were analyzed by immunoblot with antibodies to Myc or DCC intracellular domain (C-ter).

(B) Diagram showing the interaction of DCC and Robo receptor in the presence of DCC stubs. Activation of Robo by Slit leads to interaction of Robo with full-length DCC; DCC stubs are excluded from the heteroreceptor complex formed between DCC-FL and Robo, but the DCC stubs can associate with DCC-FL complex lacking Robo.

(C) Immunostaining of TAG-1-positive commissural axons in transverse sections of E12.5 mouse spinal cords. TAG-1 staining in *PS1* KO embryos was thicker at the midline (red bracket), and the ventral funiculus (yellow bracket) was absent compared to controls (WT or Het). At least six embryos were assayed for each genotype. The scale bar represents 100 μm.

(D) Model for PS1 function in axon navigation. Cellular steps in upper panels contain numbers corresponding to receptor signaling in lower panels. In wild-type spinal cords, commissural axons (red) are initially attracted to the FP by Netrin until they reach the midline and encounter repulsive Slit ligands (1). Robo becomes activated, triggering repulsion from the midline and silencing the attractive response toward Netrin through interaction with DCC (2). Thus, commissural neurons are first attracted to the FP but then grow through the midline and enter the contralateral ventral funiculus. MNs (green) differ from commissural neurons in that they also express Slits. Slit/Robo interactions in MNs prevent these cells from acquiring responsiveness to FP-derived Netrin (2). MNs may acquire responsiveness to Netrin later in development when their axons reach the periphery and Slit levels decline (1). Concomitantly, peripheral sources of Netrin could induce DCC stub production to overcome residual Slit/Robo silencing, thus triggering a response to Netrin. In *PS1* mutants, commissural axons (red) fail to exit the FP and motor axons (green) misproject toward the midline because of abnormal attraction to Netrin (3). In the absence of PS1, the sequential cleavage of DCC is disrupted leading to the accumulation of DCC stubs on the membrane that are resistant to Slit/Robo silencing, thus triggering attraction to Netrin (3). See also Figure S4.

DCC stubs dominantly bind to Robo and release full-length DCC for signaling attraction to Netrin. We performed coimmunoprecipitation assays to examine the interactions between DCC and Robo1 in the absence or presence of DCC stubs. Full-length DCC was coexpressed with myc epitope-tagged Robo1 (Robo1-Myc). γ-Secretase inhibitor was added into the cell culture bath to induce the accumulation of DCC stubs. When DCC was immunoprecipitated with an antibody to the extracellular domain of DCC (N terminus), similar amounts of Robo1 coimmunoprecipitated with DCC, regardless of whether or not DCC stubs were present (Figure 7A). Likewise, using anti-Myc antibody to immunoprecipitate Robo1, we found that coimmunoprecipitated full-length DCC pull-down was similar in the presence or absence of DCC stubs (Figure 7A). Interestingly, Robo1 immunoprecipitation did not pull down DCC stubs, suggesting these fragments of DCC are not capable of high affinity interactions with Robo1 (Figures 7A and 7B). We coprecipitated DCC stubs with full-length DCC, however, suggesting Robo1 is excluded from full-length DCC complexes containing the DCC stub (Figure 7B). Taken together, these findings indicate that the receptor complexes containing DCC stubs are insensitive to silencing because they do not interact with Robo.

Ligand Binding Induces the Accumulation of DCC Stubs

Since DCC stubs possess potent activity, we tested whether the generation and/or lifespan of this Netrin receptor fragment was regulated. After screening a variety of growth factors and neurotrophins (data not shown), we discovered that Netrin itself induced the accumulation of DCC stubs in a dose-dependent manner (Figures S4B and S4C and data not shown). A slight increase in DCC-ICD was also detected when Netrin was present, but the overall levels of full-length DCC were not substantially changed under these conditions (Figures S4B and S4C). Because DCC is sequentially cleaved by proteases, accumulation of the DCC stub intermediate could occur through one or more mechanisms, including enhancement of the metalloprotease cleavage to generate the stub and/or inhibition of γ-secretase activity involved in clearing the stub (Figure S4A). We first isolated the metalloprotease activity in this process by inhibiting γ-secretase with L-685458. Under this condition, we found DCC stub levels increased upon Netrin stimulation (Figure S4E). Next, we examined γ-secretase cleavage by comparing the ratio of DCC stub (substrate) to DCC-ICD (product) and found that DCC-ICD:DCC stub levels declined in the presence of Netrin (Figure S4D). These findings indicate that Netrin regulates the accumulation of DCC stub, likely through influencing the sequential processing of DCC mediated by metalloprotease and γ-secretase, thereby fine tuning DCC signaling (Figure S4F).

Commissural Neurons Require PS1

Although commissural neurons are initially attracted to the midline source of Netrin-1, they use Slit/Robo silencing to switch off their responsiveness in order to cross the midline. To test whether PS1 function is required for this switch, we first performed TAG-1 immunostaining of E12.5 spinal cord sections from control and *PS1* mutant embryos. TAG-1-positive commissural axons project ventrally toward the FP in both control and *PS1* mutant embryos; however, instead of forming a tightly bundled commissure at the FP, the axons appeared disorganized and defasciculated in the mutants (Figure 7C). In addition, the ventral commissure was thicker and the TAG-1 signal in the ventral funiculus was largely absent, suggesting that commissural axons had failed to exit the FP (Figure 7C). DiI labeling of dorsal commissural neurons revealed that commissural axons either stall in the FP of *PS1* mutants or inappropriately recross the midline (Figures S4G–S4L). These findings suggest that PS1 is required to switch the guidance properties of commissural neurons once they encounter the FP. In summary, PS1 plays a critical role in establishing neuronal connectivity in both efferent-motor and afferent-sensory pathways.

DISCUSSION

Long-axoned neurons grow to their targets using a series of intermediate guideposts. A classic example of an intermediate navigational target is the ventral midline of the neural tube. Commissural axons are first attracted to the FP by Netrin but then rapidly lose their responsiveness when axons encounter Slit at the midline. Slit activation of Robo receptors expressed by commissural neurons has two effects: it repels the neurons from the midline and it silences Netrin attraction (Stein and Tessier-Lavigne, 2001) (Figure 7D). Here, we show that the interplay between Robo and DCC signaling also regulates Netrin responsiveness in MNs, although there are important distinctions from the way signaling is modulated in commissural neurons. While MNs express DCC and Robo, they differ from commissural neurons in that they also express Slits (Brose et al., 1999). Slit/Robo interactions in MNs prevent these cells from acquiring responsiveness to FP-derived Netrin (Figure 7D). Thus, MNs appear to employ a self-silencing mechanism to regulate their responsiveness to Netrin, whereas commissural neurons respond to Slit produced by the FP. Here, the autonomous versus nonautonomous expression of Slit in MNs and commissural neurons, respectively, appears to underlie the difference in when and where these neurons respond to Netrin. Inside the early neural tube, Slit-positive MNs are initially insensitive to Netrin (Varela-Echavarría et al., 1997), presumably to allow their axons to extend into the periphery without becoming attracted to the midline, whereas Slit-negative dorsal commissural neurons are initially responsive to Netrin (Serafini et al., 1996). As development proceeds, Netrin expression is established in several peripheral targets of MNs, including the dermomyotome and the dorsal limb bud, and Slit expression is reduced in MNs (Holmes et al., 1998; Kennedy et al., 1994; Püschel, 1999; Serafini et al., 1996), raising the possibility that older MNs acquire responsiveness to Netrin when their axons extend to the periphery and are no longer at risk of being inappropriately attracted to the FP. By contrast, commissural neurons start to lose their Netrin responsiveness once their axons encounter Slit at the midline (Shirasaki et al., 1996; Stein and Tessier-Lavigne, 2001).

The timing and MN subtype regulation of Slit ligand expression in MNs may have a profound role in controlling guidance, counter to the typical view whereby selective guidance receptor expression is the primary determinant. Dorsally projecting cranial motor axons (cranial branchial motor neuron/cranial visceral motor neuron) not expressing Slit, show repulsion to exogenous Slit, while spinal MNs with Slit2 expression have no response (Hammond et al., 2005). This is consistent with the finding that addition of Robo1-Fc to cocultures of spinal motor explants and FP tissue does not block FP-mediated repulsion, suggesting that Slit proteins are not midline repellents for spinal MNs (Patel et al., 2001). Likewise, we found that newly generated Slit-positive MNs are insensitive to Slit repulsion, whereas more mature MNs appear to become sensitive when their Slit levels decline (Brose et al., 1999). These findings suggest that the Slits are dynamically regulated in MNs and have a variety of effects, ranging from masking repulsive responses to silencing Netrin attraction.

Although PS1 is widely expressed, it directly influences Netrin/DCC signaling with cell type precision and spatiotemporal specificity. We found that Netrin stimulation appears to activate metalloprotease activity and inhibit γ-secretase leading to accumulation of the intermediate product, DCC stubs. Although the regulatory mechanism controlling protease activity remains unclear, ligand binding to Notch receptor is thought to induce conformational changes that facilitate metalloprotease cleavage (Gordon et al., 2008). In addition, several interacting proteins and kinase pathways have been reported to modulate γ-secretase activity (De Strooper and Annaert, 2010; Kim et al., 2006). Moreover, we found that the amounts of DCC stub induced by Netrin

in MNs are normally insufficient to overcome the intrinsic silencing mediated by Slit/Robo coexpression in these cells. However, when Slit silencing is partially released, ligand-induced DCC stubs can trigger Netrin attraction (data not shown). Thus, regulation of DCC processing might help to fine tune the responsiveness of commissural neurons and MNs to Netrin (Figure 7D).

The full-length DCC receptor and membrane bound DCC stubs exhibit different protein interactions. We found that Robo interacts with the full-length DCC receptor but not the truncated DCC stubs. Thus, the differences in protein interactions of the DCC full-length and DCC stub appear to influence Slit/Robo-silencing of Netrin chemoattraction. Interestingly, a previous study showed that the myristoylated form of DCC can be coimmunoprecipitated with Robo when they are cotransfected into cells, indicating that DCC stubs might interact with Robo under some conditions (Stein and Tessier-Lavigne, 2001). We probed DCC-Robo interactions using immunoprecipitations where full-length DCC was expressed and DCC stubs were forced to accumulate with γ-secretase inhibitor. Thus, it appears that Robo interactions with DCC and its cleaved fragments are hierarchical. Full-length DCC appears to be the preferred partner of Robo, whereas the DCC stubs that accumulate with full-length receptors in *PS1* mutants escape Slit/Robo interactions that mediate silencing (Figure 7D).

Dominantly inherited mutations in the genes encoding presenilins and the amyloid precursor protein are the major causes of familial Alzheimer's disease (FAD). The prevailing view of Alzheimer's pathogenesis posits that accumulation of β-amyloid (Aβ) peptides, particularly Aβ42, is the central event triggering neurodegeneration and that FAD arises from mutations in *PS1* that alter or reduce protease activity (Hardy and Higgins, 1992; Wolfe, 2007). Our findings may provide further insight into understanding the pathogenic mechanisms that underlie FAD and help to identify treatments. First, abnormal axon guidance signaling may have roles in AD pathogenesis by affecting the maintenance and repair of neuronal circuits. Beyond guiding brain wiring during fetal development, many guidance molecules persist in the adult central nervous system and participate in maintenance, repair, and plasticity of neural circuits (Saxena and Caroni, 2007). Recent findings show that Netrin can regulate Aβ peptide production and improve Alzheimer's phenotypes in AD mouse models, which directly link Netrin signaling to neurodegeneration (Lourenço et al., 2009). Therefore, deregulation of guidance signaling by abnormal Presenilin activity may contribute to the pathogenesis and dysfunction seen in AD. Second, our observation that *PS1* mutants exhibit impaired axon growth suggests that γ-secretase inhibitors used to block toxic Aβ production in AD might disrupt axon growth leading to undesirable side effects such as impaired regeneration and repair. In the future, analysis of possible guidance abnormalities in AD mouse models may help to reveal more direct links between abnormal circuit development and the age-dependent loss of neuronal connections.

EXPERIMENTAL PROCEDURES

DNA Constructs

DCC-FL, Myr-DCC-ICD, DCC-ECD, Robo1-FL, and DN-Robo1 expression plasmids were described (Stein and Tessier-Lavigne, 2001). To generate DCC-ICD, we amplified the ICD by PCR with EcoRI and XhoI sites and cloned into HA-pcDNA3. To generate Myr-Robo1, the ICD was amplified by PCR with NheI and XmaI sites and cloned into pCAGGS-ES.

Mice

The generation of Tg (*Hb9:GFP*), Tg (*ISL^{MN}:GFP-F*), Tg (*Nestin:Cre*), *PS1$^{flox/flox}$*, *Netrin-1* mutant, *DCC* mutant, and *Robo1/2* mice was described (Fazeli et al., 1997; Lee et al., 2004; Lewcock et al., 2007; Ma and Tessier-Lavigne, 2007; Serafini et al., 1996; Shen et al., 1997; Shirasaki et al., 2006). *PS1* knockouts were generated by crossing *PS1$^{flox/flox}$* animals to mice expressing Cre in the germline. ENU screen and mapping were performed as previously described (Lewcock et al., 2007).

Explant Cultures

MNs were dissected from the spinal cords of E12 mouse embryos or electroporated chick embryos in cold neurobasal media (Invitrogen). Explants were embedded in the rat tail collagen+matrigel (1:1; BD Biosciences) and cocultured with E12 mouse FP or COS cell aggregates in MN media (Shirasaki et al., 2006) for 15–24 hr, then fixed. Where indicated, Netrin-1 proteins (R&D), Robo1-Fc chimera (1–2 μg/ml, R&D), L-685458 (1 μM, Calbiochem), and/or GM 6001 (2.5 μM, Calbiochem) were added to the culture media. Bovine serum albumin (BSA) or DMSO were used as controls. Experiments were done ≥3 times and the Student's t test was used to calculate significance.

Dunn Chamber Assay

Dunn chamber guidance assays were performed as described (Yam et al., 2009). Briefly, ISL^{MN}:GFP-labeled chick MNs were dissected, dissociated, and plated on Laminin-coated coverslips with DMSO or L-685458 (1 μM). After MNs attached (2–3 hr) and formed visible growth cones, the chambers were assembled.

SUPPLEMENTAL INFORMATION

Supplemental Information includes Supplemental Experimental Procedures and four figures and can be found with this article online at doi:10.1016/j.cell.2010.11.053.

ACKNOWLEDGMENTS

We would like to thank Edward Koo for critical reading of the manuscript, Shane Andrews for assistance with imaging, and members of the Pfaff lab for advice and discussions on the experiments and manuscript. We are also grateful to Marc Tessier-Lavigne and Jie Shen for providing *Netrin-1*, *DCC* and *PS1$^{fl/fl}$* mutant mice. We thank Roman Giger and Geetha Suresh for plasmids and Developmental Studies Hybridoma Bank for antibodies. These experiments were supported by National Institutes of Health Grant R37NS037116 through National Institute of Neurological Disorders and Stroke and the Howard Hughes Medical Institute. G.B., D.B., and K.L. are supported by the Howard Hughes Medical Institute. O.C. is supported by NINDS Grant R37NS037116. L.F. is supported by NINDS Grant P01NS031249. S.L.P. is a Howard Hughes Medical Institute Investigator.

Received: May 20, 2010
Revised: September 20, 2010
Accepted: November 8, 2010
Published: January 6, 2011

REFERENCES

Brittis, P.A., Lu, Q., and Flanagan, J.G. (2002). Axonal protein synthesis provides a mechanism for localized regulation at an intermediate target. Cell *110*, 223–235.

Brose, K., Bland, K.S., Wang, K.H., Arnott, D., Henzel, W., Goodman, C.S., Tessier-Lavigne, M., and Kidd, T. (1999). Slit proteins bind Robo receptors

and have an evolutionarily conserved role in repulsive axon guidance. Cell *96*, 795–806.

Charron, F., Stein, E., Jeong, J., McMahon, A.P., and Tessier-Lavigne, M. (2003). The morphogen sonic hedgehog is an axonal chemoattractant that collaborates with netrin-1 in midline axon guidance. Cell *113*, 11–23.

De Strooper, B., and Annaert, W. (2010). Novel research horizons for presenilins and γ-secretases in cell biology and disease. Annu. Rev. Cell Dev. Biol. *26*, 235–260.

Dickson, B.J. (2002). Molecular mechanisms of axon guidance. Science *298*, 1959–1964.

Donoviel, D.B., Hadjantonakis, A.K., Ikeda, M., Zheng, H., Hyslop, P.S., and Bernstein, A. (1999). Mice lacking both presenilin genes exhibit early embryonic patterning defects. Genes Dev. *13*, 2801–2810.

Fazeli, A., Dickinson, S.L., Hermiston, M.L., Tighe, R.V., Steen, R.G., Small, C.G., Stoeckli, E.T., Keino-Masu, K., Masu, M., Rayburn, H., et al. (1997). Phenotype of mice lacking functional Deleted in colorectal cancer (Dcc) gene. Nature *386*, 796–804.

Gitai, Z., Yu, T.W., Lundquist, E.A., Tessier-Lavigne, M., and Bargmann, C.I. (2003). The netrin receptor UNC-40/DCC stimulates axon attraction and outgrowth through enabled and, in parallel, Rac and UNC-115/AbLIM. Neuron *37*, 53–65.

Gordon, W.R., Arnett, K.L., and Blacklow, S.C. (2008). The molecular logic of Notch signaling—a structural and biochemical perspective. J. Cell Sci. *121*, 3109–3119.

Hammond, R., Vivancos, V., Naeem, A., Chilton, J., Mambetisaeva, E., Mambitisaeva, E., Andrews, W., Sundaresan, V., and Guthrie, S. (2005). Slit-mediated repulsion is a key regulator of motor axon pathfinding in the hindbrain. Development *132*, 4483–4495.

Hardy, J.A., and Higgins, G.A. (1992). Alzheimer's disease: the amyloid cascade hypothesis. Science *256*, 184–185.

Holmes, G.P., Negus, K., Burridge, L., Raman, S., Algar, E., Yamada, T., and Little, M.H. (1998). Distinct but overlapping expression patterns of two vertebrate slit homologs implies functional roles in CNS development and organogenesis. Mech. Dev. *79*, 57–72.

Kandel, E.R., Schwartz, J.H., and Jessell, T.M. (2000). Principles of neural science, Fourth Edition (New York: McGraw-Hill, Health Professions Division).

Keino-Masu, K., Masu, M., Hinck, L., Leonardo, E.D., Chan, S.S., Culotti, J.G., and Tessier-Lavigne, M. (1996). Deleted in Colorectal Cancer (DCC) encodes a netrin receptor. Cell *87*, 175–185.

Kennedy, T.E., Serafini, T., de la Torre, J.R., and Tessier-Lavigne, M. (1994). Netrins are diffusible chemotropic factors for commissural axons in the embryonic spinal cord. Cell *78*, 425–435.

Kim, S.K., Park, H.J., Hong, H.S., Baik, E.J., Jung, M.W., and Mook-Jung, I. (2006). ERK1/2 is an endogenous negative regulator of the gamma-secretase activity. FASEB J. *20*, 157–159.

Lee, S.K., Jurata, L.W., Funahashi, J., Ruiz, E.C., and Pfaff, S.L. (2004). Analysis of embryonic motoneuron gene regulation: derepression of general activators function in concert with enhancer factors. Development *131*, 3295–3306.

Lewcock, J.W., Genoud, N., Lettieri, K., and Pfaff, S.L. (2007). The ubiquitin ligase Phr1 regulates axon outgrowth through modulation of microtubule dynamics. Neuron *56*, 604–620.

Lourenço, F.C., Galvan, V., Fombonne, J., Corset, V., Llambi, F., Müller, U., Bredesen, D.E., and Mehlen, P. (2009). Netrin-1 interacts with amyloid precursor protein and regulates amyloid-beta production. Cell Death Differ. *16*, 655–663.

Ma, L., and Tessier-Lavigne, M. (2007). Dual branch-promoting and branch-repelling actions of Slit/Robo signaling on peripheral and central branches of developing sensory axons. J. Neurosci. *27*, 6843–6851.

O'Donnell, M., Chance, R.K., and Bashaw, G.J. (2009). Axon growth and guidance: receptor regulation and signal transduction. Annu. Rev. Neurosci. *32*, 383–412.

Parent, A.T., Barnes, N.Y., Taniguchi, Y., Thinakaran, G., and Sisodia, S.S. (2005). Presenilin attenuates receptor-mediated signaling and synaptic function. J. Neurosci. *25*, 1540–1549.

Parks, A.L., and Curtis, D. (2007). Presenilin diversifies its portfolio. Trends Genet. *23*, 140–150.

Patel, K., Nash, J.A., Itoh, A., Liu, Z., Sundaresan, V., and Pini, A. (2001). Slit proteins are not dominant chemorepellents for olfactory tract and spinal motor axons. Development *128*, 5031–5037.

Püschel, A.W. (1999). Divergent properties of mouse netrins. Mech. Dev. *83*, 65–75.

Saxena, S., and Caroni, P. (2007). Mechanisms of axon degeneration: from development to disease. Prog. Neurobiol. *83*, 174–191.

Selkoe, D., and Kopan, R. (2003). Notch and Presenilin: regulated intramembrane proteolysis links development and degeneration. Annu. Rev. Neurosci. *26*, 565–597.

Serafini, T., Colamarino, S.A., Leonardo, E.D., Wang, H., Beddington, R., Skarnes, W.C., and Tessier-Lavigne, M. (1996). Netrin-1 is required for commissural axon guidance in the developing vertebrate nervous system. Cell *87*, 1001–1014.

Shen, J., Bronson, R.T., Chen, D.F., Xia, W., Selkoe, D.J., and Tonegawa, S. (1997). Skeletal and CNS defects in Presenilin-1-deficient mice. Cell *89*, 629–639.

Shirasaki, R., Mirzayan, C., Tessier-Lavigne, M., and Murakami, F. (1996). Guidance of circumferentially growing axons by netrin-dependent and -independent floor plate chemotropism in the vertebrate brain. Neuron *17*, 1079–1088.

Shirasaki, R., Lewcock, J.W., Lettieri, K., and Pfaff, S.L. (2006). FGF as a target-derived chemoattractant for developing motor axons genetically programmed by the LIM code. Neuron *50*, 841–853.

Stein, E., and Tessier-Lavigne, M. (2001). Hierarchical organization of guidance receptors: silencing of netrin attraction by slit through a Robo/DCC receptor complex. Science *291*, 1928–1938.

Taniguchi, Y., Kim, S.H., and Sisodia, S.S. (2003). Presenilin-dependent "gamma-secretase" processing of deleted in colorectal cancer (DCC). J. Biol. Chem. *278*, 30425–30428.

Tessier-Lavigne, M., and Goodman, C.S. (1996). The molecular biology of axon guidance. Science *274*, 1123–1133.

Varela-Echavarría, A., Tucker, A., Püschel, A.W., and Guthrie, S. (1997). Motor axon subpopulations respond differentially to the chemorepellents netrin-1 and semaphorin D. Neuron *18*, 193–207.

Wolfe, M.S. (2007). When loss is gain: reduced presenilin proteolytic function leads to increased Abeta42/Abeta40. Talking Point on the role of presenilin mutations in Alzheimer disease. EMBO Rep. *8*, 136–140.

Yam, P.T., Langlois, S.D., Morin, S., and Charron, F. (2009). Sonic hedgehog guides axons through a noncanonical, Src-family-kinase-dependent signaling pathway. Neuron *62*, 349–362.

Yu, T.W., and Bargmann, C.I. (2001). Dynamic regulation of axon guidance. Nat. Neurosci. Suppl. *4*, 1169–1176.